ADVANCES IN ATMOSPHERIC SCIENCES, VOL. 31, SEPTEMBER 2014, 1127–1135

Mapping Near-surface Air Temperature, Pressure, Relative Humidity and Wind Speed over Mainland China with High Spatiotemporal Resolution

LI Tao[1], ZHENG Xiaogu[*1], DAI Yongjiu[1], YANG Chi[1], CHEN Zhuoqi[1], ZHANG Shupeng[1], WU Guocan[1], WANG Zhonglei[1], HUANG Chengcheng[1], SHEN Yan[2], and LIAO Rongwei[2]

[1]*College of Global Change and Earth System Science, Beijing Normal University, Beijing* 100875
[2]*National Meteorological Information Center, China Meteorological Administration, Beijing* 100081

(Received 17 September 2013; revised 31 December 2013; accepted 13 February 2014)

ABSTRACT

As part of a joint effort to construct an atmospheric forcing dataset for mainland China with high spatiotemporal resolution, a new approach is proposed to construct gridded near-surface temperature, relative humidity, wind speed and surface pressure with a resolution of 1 km×1 km. The approach comprises two steps: (1) fit a partial thin-plate smoothing spline with orography and reanalysis data as explanatory variables to ground-based observations for estimating a trend surface; (2) apply a simple kriging procedure to the residual for trend surface correction.

The proposed approach is applied to observations collected at approximately 700 stations over mainland China. The generated forcing fields are compared with the corresponding components of the National Centers for Environmental Prediction (NCEP) Climate Forecast System Reanalysis dataset and the Princeton meteorological forcing dataset. The comparison shows that, both within the station network and within the resolutions of the two gridded datasets, the interpolation errors of the proposed approach are markedly smaller than the two gridded datasets.

Key words: atmospheric forcing data, land surface model, thin-plate smoothing spline, kriging, reanalysis data

Citation: Li, T., and Coauthors, 2014: Mapping near-surface air temperature, pressure, relative humidity and wind speed over the Mainland China with high spatiotemporal resolution. *Adv. Atmos. Sci.*, **31**(5), 1127–1135, doi: 10.1007/s00376-014-3190-8.

1. Introduction

The availability of large-scale, long-term datasets of land surface water and energy budgets is essential for understanding the global environmental system and climatic change. However, historical observation records of surface evaporation, runoff, soil moisture, and soil temperature with high spatial and temporal resolution are unavailable for the majority of continental regions. Running a land surface model (LSM) to generate these variables has long been considered a good option to reconstruct historical records (e.g., Dai et al., 2003).

Meteorological forcings are required to perform off-line LSM simulations. Generally, meteorological forcings comprise seven components: near-surface air temperature, relative humidity, wind speed, downward shortwave radiation, downward longwave radiation, surface pressure, and precipitation. The actual number of forcing variables required by LSMs varies; some LSMs require less or more than these seven variables.

The importance of meteorological forcings has been demonstrated for land surface modeling efforts (Berg et al., 2003; Fekete et al., 2004; Nijssen and Lettenmaier, 2004). The results from the North American Land Data Assimilation System (NLDAS) project (Mitchell et al., 2004) indicated that first-order errors in a land surface simulation were largely due to inaccurate meteorological forcings (Pan et al., 2003; Robock et al., 2003). Other studies have also shown that land surface simulations are very sensitive to meteorological forcing accuracy (Berg et al., 2003; Fekete et al., 2004; Sheffield et al., 2004).

Until now, global atmospheric forcing datasets have mainly been derived from reanalysis datasets, such as the Climate Forecast System Reanalysis (CFSR) reanalysis dataset (Saha et al., 2010) and the Princeton forcing dataset (Sheffield et al., 2006). However, observations from approximately 200 stations only were offered by China for international exchange to construct such datasets. Therefore, their quality over the mainland of China is questionable. The spatial resolutions of these forcing datasets are primarily from $0.3^\circ \times 0.3^\circ$ to $1^\circ \times 1^\circ$. These coarse resolutions are not sufficient for catchment-scale hydrology and ecosystem studies, in which a resolution of 1 km×1 km is generally preferable.

* Corresponding author: ZHENG Xiaogu
Email: x.zheng@bnu.edu.cn

Recently, more remote sensing datasets at this resolution have become available, such as the MODIS (Moderate Resolution Imaging Spectroradiometer) LAI (leaf area index), FPAR (fraction of photosynthetically active radiation) and reflectivity products. Forcing datasets with a resolution of 1 km$\times$1 km are ideal for comparing with these remote sensing datasets.

Over the past 60 years, China has collected more 6-hourly observations than offered for international exchange. Moreover, there is a joint effort to construct an atmospheric forcing dataset for mainland China with high spatial resolution using these observations. Among these efforts, the National Meteorological Information Center of China (NMIC) primarily works on the precipitation dataset (e.g., Xie et al., 2007; Shen et al., 2010; Xie and Xiong, 2011); the Institute of Tibetan Plateau Research, Chinese Academy of Sciences (ITP-CAS) primarily works on the shortwave radiation and longwave radiation datasets (e.g., Chen et al., 2011); and the Beijing Normal University (BNU) primarily works on the near-surface air temperature, relative humidity, wind speed and surface pressure datasets. The major objectives of this study are (1) to introduce the methodology for generating a gridded near-surface temperature, relative humidity, wind speed and surface pressure dataset at a resolution of 1×1 km (named the BNU dataset) by merging ground-based observations, orography and reanalysis data; and (2) to compare the BNU dataset with other forcing datasets.

There are two popular approaches to constructing forcing datasets with high spatial resolution. The first is to fit a thin-plate smoothing spline model with the least generalized cross-validation principle (e.g., Hutchinson, 1995, 1998a, 1998b; Basher and Zheng, 1998). An advantage of this approach is that the estimation errors in sparse data locations are minimal because the least generalized cross-validation principle is applied to optimize the spline model (Wahba, 1990). However, the estimation error within the station network is often substantially larger than the observational error. In this situation, the interpolated surface often does not appear reasonable in dense data areas.

The second approach is to use a reanalysis dataset as a background field and apply a correction procedure to the background field residual (e.g., Holdaway, 1996; Alsamamra et al., 2009). An advantage of this approach is that the fitted values closely resemble the observations in dense data areas due to the correction of the residuals. However, the errors in sparse data areas are typically larger than those produced using the first approach because the selected background field provides a poorer trend surface than produced using the first approach.

In this study, a new technique that uses the first approach to modify the second is proposed. First, the trend surface is changed from the background field to one constructed by a partial thin-plate smoothing spline model with location, elevation and reanalysis data as the covariates. Then, a simple kriging is applied to the residuals. The estimates are added to the trend surface to yield the final residual-corrected surface.

The proposed approach is evaluated against the two traditional approaches. The results show that the proposed approach is indeed better than the other two algorithms; the errors are reduced in both sparse and dense data regions. The BNU dataset is also compared with the corresponding components of the CFSR and the Princeton forcing datasets. The BNU dataset estimation error is much smaller than produced from the CFSR and the Princeton forcing datasets both within the station network and on the CFSR and Princeton forcing dataset grids.

The remainder of the paper is organized as follows. The data used in the study are documented in section 2. The methodologies are described in section 3. The main results using the proposed methodologies are presented in section 4. Finally, a discussion and conclusions are given in sections 5 and 6, respectively.

2. Data

Observations at 0000, 0600, 1200 and 1800 UTC of 1.5-m near-surface air temperature, relative humidity, surface pressure and 10-m wind speed are collected from approximately 700 stations with elevation data on mainland China for the year 2003. The station locations are shown in Fig. 1. The dataset is supplied by the NMIC and is quality-controlled to maintain errors less than 2% (CMA, 2003; Ren and Xiong, 2007). For computational efficiency, the dataset is divided into four zones: west (W), mid-west (MW), northeast (NE) and southeast (SE) (see Fig. 1 for more details).

Two gridded forcing datasets are used to verify the methodology proposed in this study. The first is the CFSR dataset (Saha et al., 2010), which has a 38-km (T382; approximately $0.3125^\circ \times 0.3125^\circ$) global atmosphere resolution for 0000, 0600, 1200 and 1800 UTC. The second is the $1^\circ \times 1^\circ$ Princeton meteorological forcing dataset (Sheffield et al., 2006), which is a three-hourly dataset. However, only 0000, 0600, 1200 and 1800 UTC are used for verification purposes. In fact, the Princeton forcing dataset is interpolated to the other hours. Therefore, the data quality is not comparable to that at 0000, 0600, 1200, and 1800 UTC.

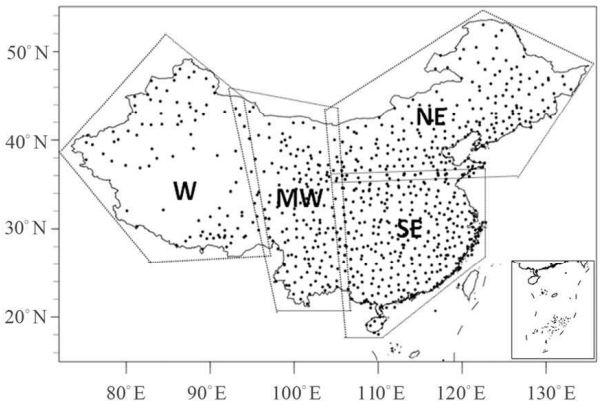

Fig. 1. Locations of stations and the division of regions over mainland China.

3. Methodology

3.1. *Estimating trend surfaces*

Every six hours, the temperature, T, is assumed to satisfy the following regression equation, which is similar to Hutchinson et al. (2009):

$$T(x) = f(x) + \alpha z(x) + \beta T_{\text{cfsr}}(x) + \varepsilon(x) \,, \tag{1}$$

where x represents a location in the domain; T_{cfsr} is the CFSR temperature; f is a two-dimensional thin-plate smoothing spline (i.e., Wahba, 1990; Zheng and Basher, 1995); z is the elevation; α and β are coefficients; and ε is the residual with zero mean and spatially invariant variance σ^2.

At each time step, Eq. (1) is trained using temperature observations, station elevations, and CFSR temperatures that are linearly interpolated from the grid points to the stations with elevation adjustment (see section 3.3.1). These data are used as input to the generalized additive model routine "gam" in the general additive model computational vehicle "mgcv" *R* statistical package (Wood, 2008, 2011; Wood et al., 2008) to derive estimated values for $\hat{f}, \hat{\alpha}, \hat{\beta}$ and $\hat{\sigma}^2$. The trend surface at any site, x, is then estimated by

$$T_t(x) = \hat{f}(x) + \hat{\alpha} z(x) + \hat{\beta} T_{\text{cfsr}}(x) \,, \tag{2}$$

where the subscript "t" stands for "trend". Specifically, for estimating the mean temperature in a 1 km grid cell, x is the center location, $z(x)$ is the mean elevation of the grid cell, and $T_{\text{cfsr}}(x)$ is the linearly interpolated CFSR temperature to x with elevation adjustment.

For the relative humidity (q), wind speed (w) and surface pressure (p), the trend surfaces are assumed to satisfy the following regression equations:

$$q(x) = f(x) + \alpha q_{\text{cfsr}}(x) + \varepsilon(x) \,; \tag{3}$$

$$w(x) = f(x) + \varepsilon(x) \,; \tag{4}$$

$$p(x) = f(x) + s(z(x)) + \varepsilon(x) \,; \tag{5}$$

where s is a one-dimensional smoothing spline function, and the other notations are the same as those in Eq. (1). The estimation procedures are the same as that for temperature.

3.2. *Residual correction*

In this study, simple kriging is applied to the residual field. For the simple kriging, the covariance between residuals $\varepsilon(x)$ and $\varepsilon(y)$, is assumed to only depend on the distance between locations x and y. Therefore, there is a one-dimensional covariance function, c, in which

$$\text{cov}(\varepsilon(x), \varepsilon(y)) = c(|x-y|) \,, \tag{6}$$

where $|x-y|$ is the Euclidean distance between locations x and y. At any location, x, the kriging estimate $\eta(x)$ is

$$\eta(x) = \begin{pmatrix} c(|x-x_1|) \\ \vdots \\ c(|x-x_n|) \end{pmatrix}^{\mathrm{T}} \begin{pmatrix} c(|x_1-x_1|) & \cdots & c(|x_1-x_n|) \\ \vdots & \ddots & \vdots \\ c(|x_n-x_1|) & \cdots & c(|x_n-x_n|) \end{pmatrix}^{-1} \begin{pmatrix} \varepsilon(x_1) \\ \vdots \\ \varepsilon(x_n) \end{pmatrix} \,, \tag{7}$$

where $x_1, \cdots, x_n$ are the observation site locations; the covariance function c in Eq. (6) is estimated using the "Krig" routine in the "fields" *R* package with input $\varepsilon(x_i), i = 1, \cdots, n$. Lastly, the residual-corrected forcing data (using temperature as an example) is defined as

$$T_{\text{c}}(x) = T_{\text{t}}(x) + \eta(x). \tag{8}$$

3.3. *Evaluation*

3.3.1. *Evaluation within the station network*

An error statistic for evaluating a methodology is the root-mean-square error (RMSE). Using temperature as an example, the RMSE is defined as

$$\text{RMSE} \equiv \sqrt{\frac{1}{N}\sum_{i=1}^{N}[\hat{T}(x_i) - T_{\text{o}}(x_i)]^2} \,, \tag{9}$$

where x_i represents a station location; N is the total number of stations in the network over a certain period; $T_{\text{o}}(x_i)$ is the observation at location x_i, and $\hat{T}(x_i)$ is an estimate at location x_i. Moreover, $\hat{T}(x_i)$ in Eq. (9) can represent the fitted trend value, $T_t(x_i)$, or the linearly interpolated value from a gridded data to location x_i. However, for gridded temperatures and pressures, the bias caused by the orographic effect between location x_i and a grid cell must be adjusted. For temperature, the gridded data are transformed to sea level using a constant lapse rate, i.e., 0.65°C (100 m)$^{-1}$. Then, the transformed gridded data at sea level are linearly interpolated to location x_i. Lastly, the interpolated temperature is transformed back from sea level to the terrain height at x_i using the same constant lapse rate. The adjustment procedure for pressure is similar. The major difference is to use the following formula:

$$p_0(x) = p(x)\left[1.0 + \frac{0.0065 z(x)}{273.15 + T(x)}\right]^{5.2568} \,, \tag{10}$$

where p and T represent the gridded pressure and temperature for transforming gridded data, $p(x)$, to sea level. Moreover,

$$p(x_i) = p_0(x_i)\left[1.0 + \frac{0.0065 z(x_i)}{273.15 + T(x_i)}\right]^{-5.2568} \,, \tag{11}$$

is used to transform the pressure at sea level, $p_0(x_i)$, back to the terrain height at x_i.

Another error statistic for evaluating a methodology is cross validation (CV), i.e.,

$$\text{CV} \equiv \sqrt{\frac{1}{N}\sum_{i=1}^{N}[\hat{T}_{-i}(x_i) - T_{\text{o}}(x_i)]^2} \,, \tag{12}$$

where $\hat{T}$ represents T_{t} or T_{c} and the subsctript $-i$ indicates that the value is estimated using all observations in the network except the observation $T_{\text{o}}(x_i)$.

Both the RMSE and CV represent the goodness of fit. However, observation $T_o(x_i)$ is included for estimating the value at x_i in the RMSE, but this is not the case for CV. The RMSE represents the fitted error in dense data areas, while CV is used to assess the generality of statistical analysis results to an independent dataset.

3.3.2. *Evaluation on the grid*

The reduced variance of the newly estimated temperature compared with the CFSR temperature can be estimated as (see Appendix)

$$\sqrt{\frac{1}{M}\sum_{m=1}^{M}[T_{\mathrm{cfsr}}(m)-T_o(m)]^2-\frac{1}{M}\sum_{m=1}^{M}[T_{-m}(m)-T_o(m)]^2}\ , \tag{13}$$

where m is a grid cell which contains observations; M is the total number of these grid cells; $T_o(m)$ is the observed mean within m; $T_{\mathrm{cfsr}}(m)$ is the CFSR data in m; and $T_{-m}(m)$ is the mean of the trend surface at the 1-km sub-grid centers within m using all observations in the network except observations within m.

4. Results

To verify the usefulness of the CFSR temperature and relative humidity dataset in producing a trend surface, spline CVs [Eqs. (1) and (3)] are shown in the second rows of Tables 1 and 2, respectively. The results show that the spline CVs with the CFSR data as a covariate are smaller than the splines without the CFSR data as a covariate. This finding suggests that the CFSR dataset has moderate contributions to the temperature and relative humidity forcing fields.

To verify the usefulness of the CFSR wind speed and surface pressure dataset in producing trend surfaces, the CFSR data are added to Eq. (4) and Eq. (5), i.e.,

$$w(x)=f(x)+\alpha w_{\mathrm{cfsr}}(x)+\varepsilon(x)\ , \tag{14}$$

and

$$p(x)=f(x)+s(z(x))+\alpha p_{\mathrm{cfsr}}(x)+\varepsilon(x)\ . \tag{15}$$

The spline CVs [Eqs (14) and (15)] are shown in the second rows of Tables 3 and 4, respectively. The results show that using the CFSR data as a covariate does not reduce the CVs. These facts suggest that the CFSR dataset has no contribution to the pressure and wind speed forcing fields.

The simple kriging method specified in section 3.2 is applied to the residual, $\varepsilon(x)$, in Eq. (1) and Eqs. (3)–(5). The corresponding results are also listed in the third rows of Tables 1–4, respectively. For temperature and relative humidity, the spline model CVs with residual correction are smaller than those without residual correction. This finding suggests that the correction method is effective for the temperature and relative humidity. However, for the pressure and wind speed, the spline model CVs with residual correction and the trend surface are the same, indicating that the residual correction is unnecessary for the pressure and the wind speed forcing fields.

Table 1. Cross validation [Eq. (12)] of air temperature (°C) for the zones and the spline model Eq. (1) with or without CFSR reanalysis data as covariant and with or without residual Kriging. W: West, MW: Middle West, NE: North East, SE: South East.

With CFSR reanalysis as covariate?	Residual Kriging applied?	W zone	MW zone	NE zone	SE zone	All zone
No	No	2.96	2.09	1.88	1.49	2.10
Yes	No	2.80	2.04	1.82	1.41	2.02
Yes	Yes	2.76	2.01	1.78	1.34	1.97

Table 2. Similar to Table 1, but for relative humidity (%) and Eq. (3).

With CFSR reanalysis as covariate?	Residual Kriging applied?	W zone	MW zone	NE zone	SE zone	All zone
No	No	14.72	11.83	10.49	9.11	11.54
Yes	No	14.12	11.54	10.25	8.91	11.20
Yes	Yes	14.07	11.40	10.03	8.75	11.06

Table 3. Similar to Table 1, but for wind speed (m s^{-1}) and Eq. (4).

With CFSR reanalysis as covariate?	Residual Kriging applied?	W zone	MW zone	NE zone	SE zone	All zone
No	No	0.52	0.51	0.48	0.53	0.51
Yes	No	0.52	0.51	0.48	0.53	0.51
Yes	Yes	0.52	0.51	0.48	0.53	0.51

Table 4. Similar to Table 1, but for surface pressure (hPa) and Eq. (5).

With CFSR reanalysis as covariate?	Residual Kriging applied?	W zone	MW zone	NE zone	SE zone	All zone
No	No	1.78	1.75	1.15	1.17	1.46
Yes	No	1.78	1.75	1.15	1.17	1.46
Yes	Yes	1.78	1.75	1.15	1.17	1.46

5. Discussion

5.1. *Comparison to the CFSR and Princeton datasets*

The CFSR reanalysis and Princeton forcing datasets are perhaps the two most popular atmospheric forcing datasets for LSMs. In this section, these two datasets are compared with the BNU dataset in the observation network and on a grid with a spatial resolution analogous to the CFSR and Princeton forcing datasets.

5.1.1. *Within the observation network*

In practical applications, coarse-resolution meteorological forcing datasets are typically further interpolated onto

a fine-resolution grid (e.g., Shi et al., 2011). Therefore, it is useful to validate the interpolated CFSR and Princeton datasets within the station network. The gridded CFSR data are linearly interpolated to the observation sites; the elevation adjustments are performed for the temperature and pressure fields (as described in section 3.3.1). The corresponding RMSEs for the temperature, relative humidity, wind speed and surface pressure are listed in Table 5. The corresponding spline CVs are much larger, especially for the wind speed and surface pressure fields.

Similarly, the Princeton forcing dataset is also linearly interpolated to the observation sites; the corresponding RMSEs for temperature, relative humidity, wind speed and surface pressure are listed in Table 6. For temperature, relative humidity and wind speed, the Princeton forcing dataset RMSEs are larger than for the CFSR forcing data. However, this finding is not surprising because the CFSR forcing dataset spatial resolution is 0.3125°, while the Princeton forcing dataset spatial resolution is 1°. It is surprising that the CFSR surface pressure RMSE is much larger than for the Princeton forcing dataset. This finding requires further investigation.

Overall, the spline CVs (the second rows in Tables 1 and 2 and the first rows in Tables 3 and 4) are much smaller than the RMSEs for both the CFSR and Princeton forcing datasets, indicating that the BNU dataset is better than these two gridded datasets within the observation network. Moreover, simple kriging is applied on the residual fields for trend surface correction in the BNU dataset. Then, the true BNU dataset interpolation errors at the grid points nearest the observation sites are even smaller.

5.1.2. *On the grid*

To verify whether the BNU product is better than the CFSR data on the 0.3125° grid (the CFSR dataset resolution), the square root of the reduced variances for the BNU forcing data over the CFSR reanalysis data [Eq. (13)] are calculated and listed in Table 7. Table 7 shows that these values are all positive and larger than the spline CVs listed in the second rows of Tables 1 and 2 and in the first rows of Tables 3 and 4. This finding indicates that the BNU dataset at the CFSR dataset resolution is much more accurate than the CFSR dataset. The difference maps of interpolated meteorological data and reanalysis data at 0200LST 3 January and 1400LST 3 July are shown in Fig. 2.

Similarly, the square root of the reduced variances for the BNU forcing data compared with the Princeton forcing data are calculated and listed in Table 8. The results indicate that the BNU forcing data at the Princeton forcing dataset resolution is also much more accurate than the Princeton forcing dataset.

5.2. *Discussion on the methodology*

5.2.1. *Elevation*

Temperature and pressure are sensitive to elevation. For temperature, the elevation covariate coefficient [α in Eq. (1)] is an empirically determined, regionally averaged lapse rate (Hutchinson, 1991). The daily average estimated lapse rates are shown in Fig. 3, demonstrating a pronounced seasonal pattern with higher lapse rates during summer. This finding coincides with the results of Rolland (2003), Blandford et al. (2008) and Hutchinson et al. (2009) and indicates that if a constant lapse rate is used in Eq. (1), the estimated surface temperature accuracy decreases. To confirm this idea, a comparative test is performed for zone W from January to March because the daily lapse rates during this period are much lower than 0.65°C (100 m)$^{-1}$. First, the NMIC observations and CFSR temperature data are transformed to sea level using a constant lapse rate of 0.65°C (100 m)$^{-1}$. Then, the trend surface is estimated using Eq. (1) without the covariate *z*. Lastly, the estimated surface value is transformed back to the terrain height using the same constant lapse rate. The corresponding CV is 4.35°C, which is larger than the CV of the newly proposed method (4.03°C). The proposed elevation adjustment approach [Eq. (1)] is also tested against the

Table 5. RMSE of CFSR dataset.

	W zone	MW zone	NE zone	SE zone	All zone
Temperature (°C)	4.23	3.47	2.97	2.40	3.27
Humidity (%)	22.48	19.50	18.42	14.41	18.70
Wind speed (m s^{-1})	3.44	2.90	3.24	2.48	3.10
Pressure (hPa)	26.66	19.93	9.73	10.07	16.75

Table 6. RMSE of the Princeton dataset.

	W zone	MW zone	NE zone	SE zone	All zone
Temperature (°C)	5.40	4.08	4.33	3.34	4.29
Humidity (%)	25.27	21.91	21.26	16.34	21.19
Wind speed (m s^{-1})	3.61	3.17	3.17	2.28	3.19
Pressure (hPa)	4.07	3.91	4.00	4.18	4.04

Table 7. The square root of the reduced variances of BNU forcing data over CFSR reanalysis data [Eq. (13)].

	W zone	MW zone	NE zone	SE zone	All zone
Temperature (°C)	4.48	3.53	2.39	2.12	3.14
Humidity (%)	17.60	16.02	15.48	11.12	15.16
Wind speed (m s^{-1})	3.40	2.85	3.20	2/42	3.06
Pressure (hPa)	39.79	32.55	14.75	19.05	26.79

Table 8. The same as Table 7, but for Princeton forcing data.

	W zone	MW zone	NE zone	SE zone	All zone
Temperature (°C)	4.69	3.11	4.00	2.84	3.71
Humidity (%)	20.52	18.42	18.80	13.45	17.83
Wind speed (m s^{-1})	3.53	3.11	3.08	2.71	3.11
Pressure (hPa)	11.56	3.88	8.88	3.79	8.09

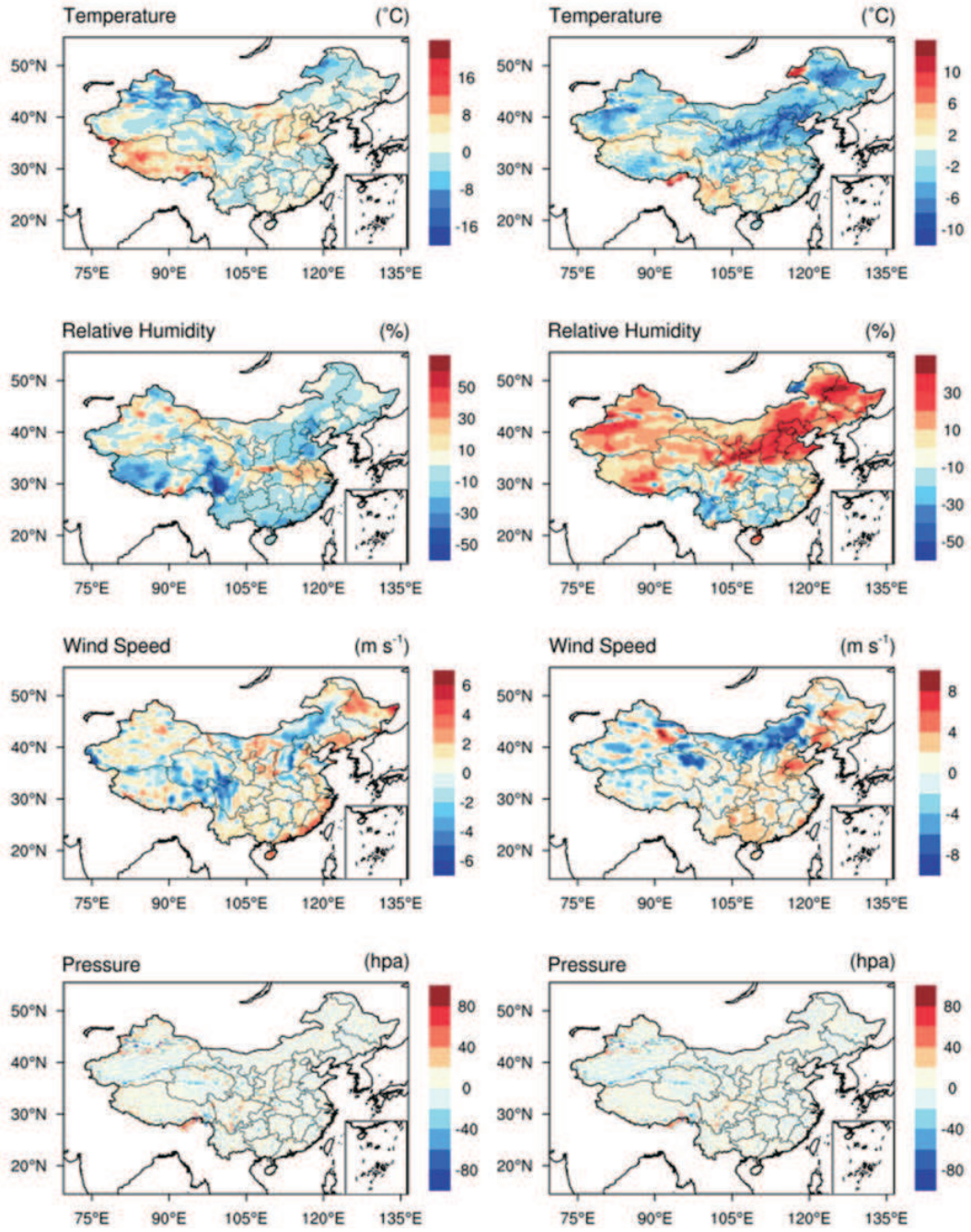

Fig. 2. Maps of differences between interpolated meteorological data and CFSR reanalysis data at 0200 LST 3 January 2003 (left panel) and 1400 LST 3 July 2003 (right panel).

traditional algorithm in other seasons and zones. The results show that the newly proposed adjustment approach continually produces smaller CVs than the traditional adjustment approach. However, zone W produces the largest decrease in CV from January to March.

A similar comparative test is also performed for pressure in zone W from January to March in 2003. First, the pressure at observation site x is transformed to sea level using Eq. (10). Then, the sea level trend surface is constructed using Eq. (5) without the one-dimensional spline, $s(z)$. Lastly, the trend surface is transformed back to the terrain height using Eq. (11). The resulting CV is 3.92 hPa, which is larger than the CV estimated using Eq. (5) (1.46 hPa).

From the aforementioned comparative tests, the temperature trend surface estimated using the newly proposed methodology is better than the surface derived using a constant lapse rate. A lapse rate of $0.65^{\circ}\mathrm{C}\ (100\ \mathrm{m})^{-1}$ can approximately reflect the temperature–elevation relationship. However, the fixed value remains inadequate to accurately represent the temperature field. This finding is also true for the pressure–elevation relationship presented in Eqs. (10) and (11).

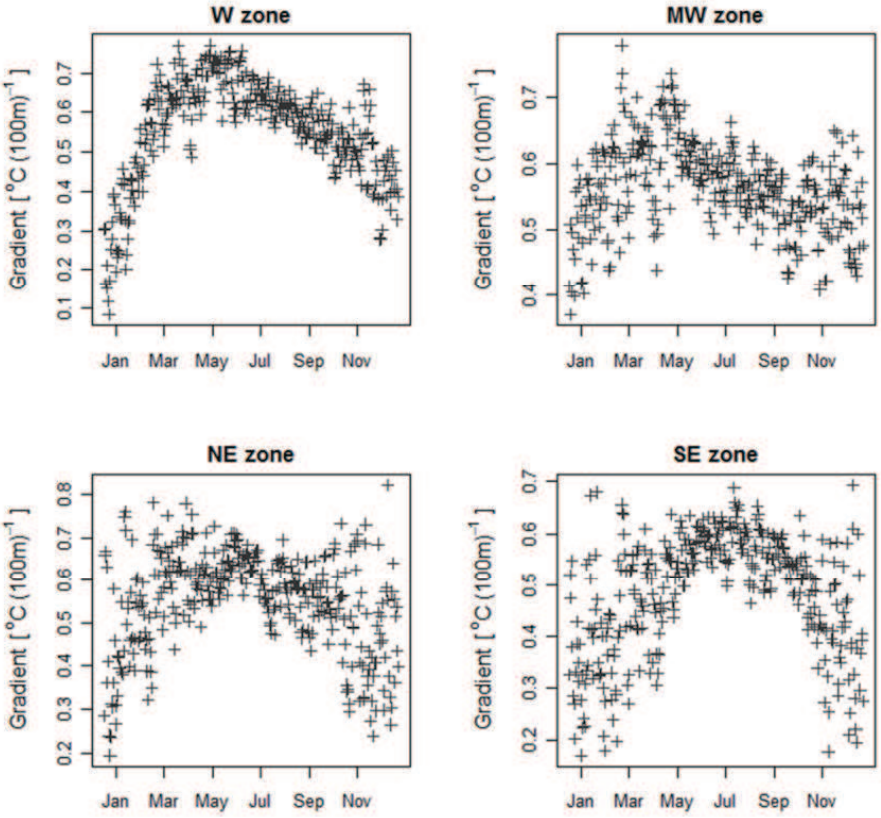

Fig. 3. Estimated daily average lapse rate for temperature [$-\alpha$ in Eq. (1)].

5.2.2. *Trend surface quality*

The Princeton dataset (as the background field) is used to demonstrate the importance of trend surfaces for the final product. A simple kriging procedure is applied to the residual field for further correction. The estimated CVs for this method are 3.4°C, 15.9%, 1.3 m s^{-1} and 3.9 hPa for temperature, relative humidity, wind speed and surface pressure, respectively. These CVs are smaller than those without residual corrections (Table 6), indicating that the residual correction is effective. However, these CVs remain larger than those from the newly proposed method (the third rows in Tables 1–4). This finding is because the spline CVs are much smaller than the Princeton dataset RMSE. Therefore, a higher quality trend surface can lead to a better-corrected surface.

Recently, a new dataset was developed by ITPCAS using the same observations that are implemented in this study (He, 2010; Chen et al., 2011). The CVs using their methodology are 2.50°C, 12.28%, 0.76 m s^{-1} and 3.06 hPa for near-surface temperature, relative humidity, wind speed and surface pressure, respectively, which are moderately larger than the CVs proposed in this study, i.e., 1.97°C, 11.06%, 0.51 m s^{-1} and 1.46 hPa, respectively. There may be several reasons for these differences. For example, that ITPCAS methodology does not use reanalysis data as a covariate, perform trend surface correction, or adopt the elevation adjustment approaches for temperature and pressure documented in section 3.3.1. Moreover, the ITPCAS methodology uses the Princeton forcing dataset to determine the trend surfaces.

The trivariate thin-plate smoothing spline with elevation as the third independent variable has been demonstrated as a better approach than the bivariate thin-plate smoothing spline for some datasets [e.g., maximum and minimum temperatures in Canada (Hutchinson et al., 2009)]. This point is tested using the temperature dataset for mainland China. The CVs for the partial trivariate spline with CFSR data as the covariate are 3.01°C, 2.24°C, 1.92°C and 1.40°C for zones W, MW, NE and SE, respectively. These CVs are larger than the bivariate spline CVs shown in the second row of Table 1 except for zone SE where the two CVs are nearly identical. These differences may be because the temperature datasets for zones W, MW and NE are not sufficiently dense. Potentially, the trivariate spline function can model the lapse rate spatial variability (Hutchinson et al., 2009). However, the observation sites in zones W, MW and NE may be too sparse to measure this spatial variability well. Therefore, a simpler model is more preferable. Moreover, the observation sites in zone SE are denser than in the other three regions. Therefore, the trivariate spline and partial bivariate spline provide similar fits to the data. If the data were denser, the trivariate spline would fit the data better.

5.2.3. *Residual correction*

Fitting a smoothing spline can cause the residuals to be substantially larger than the observation error range, i.e., the estimation error in dense data areas is too large. In this situa-

Table 9. RMSE of the BNU dataset.

	W zone	MW zone	NE zone	SE zone	All zone
Temperature (°C)	2.24	1.69	1.54	1.23	1.68
Humidity (%)	11.25	9.81	8.93	8.00	9.50
Pressure (hPa)	1.21	1.48	0.96	0.99	1.16
Wind speed (m s^{-1})	0.48	0.48	0.44	0.50	0.48

tion, the interpolated surface often appears physically unreasonable in dense data areas. Unfortunately, this is the case for the temperature (average RMSE of 1.68°C) and relative humidity (average RMSE of 9.50%) fields in this study (Table 9). Therefore, residual correction is necessary and produces reasonable results.

Generally, the residual field estimated using the smoothing spline model is assumed to be statistically and spatially independent. Therefore, a simple kriging correction procedure seems unhelpful. However, this is often not the case in practice, which is possibly related to the trend surface quality. For a relatively poor trend surface, the residuals are substantially larger than the observation error range, such as for the temperature and relative humidity fields. Therefore, the residual fields may also contain some information that should belong to the trend surfaces. This error may result in a correlated residual field. Therefore, residual correction is necessary. This study on the temperature and relative humidity fields supports this framework.

6. Conclusions

In this study, a new approach for generating near-surface temperature, relative humidity, wind speed and pressure fields is proposed. The proposed approach is applied to the NMIC observations and the CFSR reanalysis dataset for mainland China to generate a six-hourly 1-km gridded dataset. The error in the constructed dataset using the proposed scheme is smaller than the CSFR and Princeton meteorological forcing dataset errors, both within the station network and on the CFSR and Princeton dataset grids.

This study is the first practical attempt at fitting a partial thin-plate smoothing spline with reanalysis data as a covariate to ground-based observations for generating a trend surface. Moreover, this study is the first to suggest the importance of using a residual kriging procedure to correct trend surfaces estimated using smoothing spline models. It is further suggested that a better trend surface can be derived by carefully selecting spline model covariates.

Lastly, the proposed approach is applied to generate surface temperature, relative humidity, pressure, wind speed and precipitation at 1-km and three-hourly resolutions from 1958 to 2010 over mainland China. The dataset is available on request or downloadable from http://globalchange.bnu.edu.cn/.

Acknowledgements. This work was supported by the National Program on Key Basic Research Project of China (Grant Nos. 2010CB951604 and 2010CB950703), the National Natural Science Foundation of China General Program (Grant Nos. 40975062 and 40875062), R&D Special Fund for Nonprofit Industry (Grant No. Meteorology GYHY201206008), the Key Technologies Research and Development Program of China (Grant No. 2013BAC05B04), and the Fundamental Research Funds for the Central Universities (Grant No. 2012LYB42). We thank Dr. XIONG Anyuan for technical help and moral encouragement. We also would like to thank Drs. YANG Kun and Carsten FREDERIKSEN for their valuable comments.

APPENDIX

Proof of Eq. (13)

Let $T(m)$ be the true temperature value in grid m, and suppose CFSR error, $T_{\rm cfsr}(m)-T(m)$, and observation error, $T_{\rm o}(m)-T(m)$, are statistically independent. Then,

$$\frac{1}{M}\sum_{m=1}^{M}[T_{\rm cfsr}(m)-T_{\rm o}(m)]^2 \approx \frac{1}{M}\sum_{m=1}^{M}[T_{\rm cfsr}(m)-T(m)]^2+\frac{1}{M}\sum_{m=1}^{M}[T(m)-T_{\rm o}(m)]^2 .$$

Similarly,

$$\frac{1}{M}\sum_{m=1}^{M}[T_{-m}(m)-T_{\rm o}(m)]^2 \approx \frac{1}{M}\sum_{m=1}^{M}[T_{-m}(m)-T(m)]^2+\frac{1}{M}\sum_{m=1}^{M}[T(m)-T_{\rm o}(m)]^2 .$$

Therefore,

$$\frac{1}{M}\sum_{m=1}^{M}[T_{\rm cfsr}(m)-T(m)]^2-\frac{1}{M}\sum_{m=1}^{M}[T_{-m}(m)-T(m)]^2 \approx \frac{1}{M}\sum_{m=1}^{M}[T_{\rm cfsr}(m)-T_{\rm o}(m)]^2-\frac{1}{M}\sum_{m=1}^{M}[T_{-m}(m)-T_{\rm o}(m)]^2 .$$

REFERENCES

Alsamamra, H., J. A. Ruiz-Arias, D. Pozo-Vázquez, and J. Tovar-Pescador, 2009: A comparative study of ordinary and residual kriging techniques for mapping global solar radiation over southern Spain. *Agricultural and Forest Meteorology*, **149**, 1343–1357.

Basher, R. E., and X.G. Zheng, 1998: Mapping rainfall fields and their ENSO variation in data-sparse tropical south-west Pacific Ocean region. *Int. J. Climatol.*, **18**, 237–251.

Berg, A. A., J. S. Famiglietti, J. P. Walker, and P. R. Houser, 2003: Impact of bias correction to reanalysis products on simulations of North American soil moisture and hydrological fluxes. *J. Geophys. Res.*, **108**, 4490, doi: 10.1029/2002JD 003334.

Blandford, T. R., K. S. Humes, B. J. Harshburger, B. C. Moore, and V. P. Walden, 2008: Seasonal and synoptic variations in near-surface air temperature lapse rates in a mountainous basin. *J. Appl. Meteor. Climatol.*, **47**, 249–261, doi: 10.1175/2007 JAMC1565.1.

Chen, Y., K. Yang, J. He, J. Qin, J. Shi, J. Du, and Q. He, 2011: Improving land surface temperature modeling for dry land of China. *J. Geophys. Res.*, **116**, D20104, doi: 10.1029/2011JD015921.

CMA, 2003: *Specification of Surface Meteorological Observation*. Meteorological Press, 151 pp. (in Chinese)

Dai, Y., and Coauthors, 2003: The command land model. *Bull. Amer. Meteor. Soc*., **84**, 1013–1023.

Fekete, B. M., C. J. Vörösmarty, J. O. Roads, and C. J. Willmott, 2004: Uncertainties in precipitation and their impacts on runoff estimates. *J. Climate*, **17**, 294–304.

He, J., 2010: Development of surface meteorological dataset of China with high temporal and spatial resolution. M.S. thesis, Inst. of Tibetan Plateau Res., Chin. Acad. of Sci., Beijing, China, 78 pp.

Holdaway, M. R., 1996: Spatial modeling and interpolation of monthly temperature using kriging. *Climate Research*, **6**, 215–225.

Hutchinson, M. F., 1991: The application of thin plate splines to continent-wide data assimilation. *Data Assimilation Systems*, J. D. Jasper, BMRC Research Report No.27, Bureau of Meteorology, Melbourne, 104–113.

Hutchinson, M. F., 1995: Interpolating mean rainfall using thin plate smoothing splines. *International Journal of Geographical Information Science*, **9**, 385–403.

Hutchinson, M. F., 1998a: Interpolation of rainfall data with thin plate smoothing splines. Part I: Two dimensional smoothing of data with short range correlation. *Journal of Geographic Information and Decision Analysis*, **2**, 153–167.

Hutchinson, M. F., 1998b: Interpolation of rainfall data with thin plate smoothing splines. Part II: Analysis of topographic dependence. *Journal of Geographic Information and Decision Analysis*, **2**, 168–185.

Hutchinson, M. F., D. W. McKenney, K. Lawrence, J. H. Pedlar, R. F. Hopkinson, E. Milewska, and P. Papadopol, 2009: Development and testing of Canada-Wide interpolated spatial models of daily minimum-maximum temperature and precipitation for 1961–2003. *J. Appl. Meteor. Climatol.*, **48**, 725–741, doi: 10.1175/2008JAMC1979.1.

Mitchell, K. E., and Coauthors, 2004: The multi-institution North American land data assimilation system (NLDAS): Utilizing multiple GCIP products and partners in a continental distributed hydrological modeling system. *J. Geophys. Res.*, **109**, D07S90, doi: 10.1029/2003JD003823.

Nijssen, B., and D. P. Lettenmaier, 2004: Effect of precipitation sampling error on simulated hydrological fluxes and states: Anticipating the global precipitation measurement satellites. *J. Geophys. Res.*, **109**, D02103, doi: 10.1029/2003JD003497.

Pan, M., and Coauthors, 2003: Snow process modeling in the North American land data assimilation system (NLDAS): 2. Evaluation of model simulated snow water equivalent. *J. Geophys. Res*., **108**, 8850, doi: 10.1029/2003JD003994.

Ren, Z. H., and A. Y. Xiong, 2007: Operational system development on three-step quality control of observations from AWS. *Meteorological Monthly*, **33**(1), 19–24. (in Chinese)

Robock, A., and Coauthors, 2003: Evaluation of the North American land data assimilation system over the southern Great Plains during the warm season. *J. Geophys. Res*., **108**, 8846, doi: 10.1029/2002JD003245.

Rolland, C., 2003: Spatial and seasonal variations of air temperature lapse rate in alpine regions. *J. Climate.*, **16**, 1032–1046.

Saha, S., and Coauthors, 2010: The NCEP climate forecast system reanalysis. *Bull. Amer. Meteor. Soc.*, **91**, 1015–1057. doi: 10.1175/2010BAMS3001.1.

Sheffield, J., A. D. Ziegler, E. F. Wood, and Y. Chen, 2004: Correction of the high-latitude rain day anomaly in the NCEP-NCAR reanalysis for land surface hydrological modeling. *J. Climate*, **17**, 3814–3828.

Sheffield, J., G. Goteti, and E. F. Wood, 2006: Development of a 50-year high-resolution global dataset of meteorological forcings for land surface Modeling. *J. Climate*, **19**, 3088–3111.

Shen, Y., A. Y. Xiong, Y. Wang, and P. P. Xie, 2010: Performance of high-resolution satellite precipitation products over China. *J. Geophys. Res.*, **115**, D02114, doi: 10.1029/2009JD012097.

Shi, C. X., Z. H. Xie, H. Qian, M. L. Liang, and X. C. Yang, 2011: China land soil moisture EnKF data assimilation based on satellite remote sensing data. *Science China–Earth Sciences*, **54**, 1430–1440, doi: 10.1007/s11430-010-4160-3.

Wahba, G., 1990: *Spline Models for Observational Data*. Vol. 59, *CBMS-NSF Regional Conference Series in Applied Mathematics*, SIAM, 169 pp.

Wood, S. N., 2008: Fast stable direct fitting and smoothness selection for generalized additive models. *Journal of the Royal Statistical Society: Series B* (*Statistical Methodology*), **70**, 495–518.

Wood, S. N., 2011: Fast stable restricted maximum likelihood and marginal likelihood estimation of semiparametric generalized linear models. *Journal of the Royal Statistical Society: Series B* (*Statistical Methodology*), **73**, 3–36.

Wood, S. N., M. V. Bravington, and S. L. Hedley, 2008: Soap film smoothing. *Journal of the Royal Statistical Society: Series B* (*Statistical Methodology*), **70**, 931–955.

Xie, P. P., M. Chen, S. Yang, A. Yatagai, T. Hayasaka, Y. Fukushima, and C. Liu, 2007: A gauge-based analysis of daily precipitation over East Asia. *J. Hydrometeor.*, **8**(3), 607–626.

Xie, P. P., and A. Y. Xiong, 2011: A conceptual model for constructing high-resolution gauge-satellite merged precipitation analyses. *J. Geophys. Res*., **116**(D21), D21106, doi: 10.1029/2011JD016118.

Zheng, X., and R. E. Basher, 1995: Thin-plate smoothing spline modeling of spatial climate data and its application to mapping south pacific rainfalls. *Mon. Wea. Rev.*, **123**, 3086–3102.